Interplay between Static and Dynamic Properties of Semifluxons in $YBa_2Cu_3O_{7-\delta}$ 0-π Josephson Junctions

K. Cedergren,[1] J. R. Kirtley,[2] T. Bauch,[1] G. Rotoli,[3] A. Troeman,[4] H. Hilgenkamp,[4] F. Tafuri,[5] and F. Lombardi[1]

[1]*Quantum Device Physics Laboratory, Department of Microtechnology and Nanoscience, Chalmers University of Technology, SE-412 96 Göteborg, Sweden*

[2]*Center for Probing the Nanoscale, Stanford University, Stanford, California 94304, USA*

[3]*CNISM and DIMEG, Università di L'Aquila, Località Monteluco, 67040 L'Aquila, Italy*

[4]*Faculty of Science and Technology and MESA+ Institute for Nanotechnology, University of Twente, Post Office Box 217, 7500 AE Enschede, The Netherlands*

[5]*Dipartimento Ingegneria dell'Informazione, Seconda Università di Napoli e CNR-SPIN, Aversa (CE), Italy*

(Received 18 November 2009; published 28 April 2010)

We have investigated the static and dynamic properties of long $YBa_2Cu_3O_{7-\delta}$ 0-π Josephson junctions and compared them with those of conventional 0 junctions. Scanning SQUID microscope imaging has revealed the presence of a semifluxon at the phase discontinuity point in 0-π Josephson junctions. Zero field steps have been detected in the current-voltage characteristics of all junctions. Comparison with simulation allows us to attribute these steps to fluxons traveling in the junction for conventional 0 junctions and to fluxon-semifluxon interactions in the case of 0-π Josephson junctions.

DOI: 10.1103/PhysRevLett.104.177003 PACS numbers: 85.25.Cp

Josephson circuitry with intrinsic π shifts in the superconducting quantum mechanical phase [1–4], although originally predicted for junctions with magnetic interactions in the barrier region (π junctions) [1], were first demonstrated experimentally in devices that depended on momentum dependent π-phase shifts within high temperature superconductors (HTS) [5,6]. Such devices have been used to demonstrate *d*-wave pairing symmetry in the HTS [5,6] as well as for simplified rapid single flux quantum (RSFQ) logic [7]. In loops with an odd number of π-phase shifts (π rings) and Josephson junctions with π steps along them (0-π junctions) [8–11], spontaneous currents are induced to compensate for the π-phase shift, generating a semifluxon with (in the limit of high ring inductance or long junction length) a half-flux quantum of magnetic flux [6,12,13]. A semifluxon represents the ground state of the system and is therefore less sensitive to environmental fluctuations compared to ordinary fluxons in long Josephson junctions [14]. These properties can be exploited to engineer semifluxon-based devices for information processing and memories both in the classical and quantum regime.

Most of the research on semifluxon physics has been performed with HTS JJs; this work has motivated a new interest in superconductor-ferromagnet-superconductor Josephson π junctions [2,3,15–17]. The research in this area has centered on the static arrangement of semifluxons in long 0-π JJs or arrays [18,19]. Signatures of semifluxon dynamics have been reported in low dissipation 0-π JJs obtained by engineering LTS junctions with a ferromagnetic and insulating barrier [20] and by a standard Nb-AlO_x-Nb technology where a pair of current injectors creates an artificial 0-π discontinuity [21]. These works have not directly proven the existence of a static semifluxon at the discontinuity point, fundamental for applications in quantum information processing and storage.

This Letter provides a direct correlation between the static and dynamic properties of a semifluxon in the same 0-π Josephson devices. We have fabricated all HTS $YBa_2Cu_3O_{7-\delta}$ (YBCO) corner 0-π junctions using the biepitaxial technique, and we have performed transport and scanning SQUID (superconducting quantum interference device) microscopy (SSM) measurements on the same samples. These experiments are difficult due to the severe requirements on the junction parameters: there must be both sufficiently high values of the critical current and symmetry of the 0 and π facet to induce a semifluxon, and sufficiently low dissipation to observe semifluxon dynamics. We have found the proper window of junction parameters to satisfy both requirements. Starting from the current—voltage characteristics of the junctions and the magnetic-field dependence of the Josephson currents, we have been able to reconstruct, through simulations, the dynamics of the specific junctions.

For fabrication of the samples, we use the biepitaxial technique, described in more detail in [22,23], in which one electrode of the grain boundary junction is formed by (103) YBCO and the other by (001) YBCO. The (001) YBCO has an in-plane rotation of 45° with respect to the [001] in-plane direction of the (110) $SrTiO_3$ (STO) substrate. Because of this rotation, one of the facets in a corner shaped junction will have a shift of π of the superconductive phase compared to the other (see Fig. 1).

The total length of each junction is 10 μm and the thickness of the YBCO is 160 nm. We have patterned, on the same sample, 0-π junctions with various grain boundary (GB) angles θ, where θ is the angle between the GB line and the [001] in-plane direction of the STO substrate.

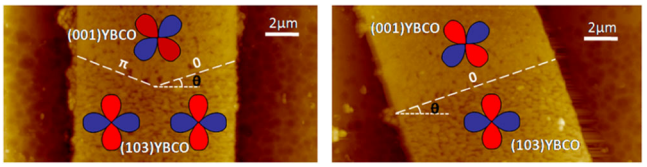

FIG. 1 (color online). Atomic force micrographs of the 0-π (left panel) and the 0 junctions (right panel) presented here. The orientation of the order parameter in the two electrodes is shown.

For each 0-π junction, there is a reference 0 junction with the same GB angle.

Figure 2 shows the critical current versus magnetic field for one of the 0-π junctions and its corresponding reference 0 junction, with a GB angle of 20°. Since the π phase shift in one facet of the 0-π junction corresponds to a negative critical current at zero magnetic field, we expect a minimum for the total critical current in the limit $L < 10\lambda_J$ [19] compared to a maximum for a 0 junction. The reduced but nonzero critical current at zero applied magnetic field (Fig. 2 left panel) is typical for a 0-π junction in a moderately long regime [19], consistent with our calculated Josephson penetration depth λ_j of 3 μm at a temperature $T = 4.2$ K, leading to L/λ_j of the order of 3, where L is the total length of the two facets. The value for λ_j has been obtained by assuming a) that the London penetration depth λ_L is 2 μm in the c-axis direction and 150 nm in the a-b planes, consistent with a critical temperature of 89 K for our YBCO film [24] and b) by considering that for a GB angle of 20° the effective London penetration depth in the (103) film is of the order of 500 nm from geometrical arguments [25]. For comparison, Fig. 2, right panel, shows an almost ideal Fraunhofer field dependence for the "0" reference junction.

We used scanning SQUID microscopy to establish that spontaneous nucleation of semifluxons occurs in the 0-π junctions. Our SQUID sensor had an integrated pickup loop with an effective pickup area of 10–15 μm^2. We have investigated both reference "0" and "0-π" junctions. SSM imaging of these junctions was difficult because the

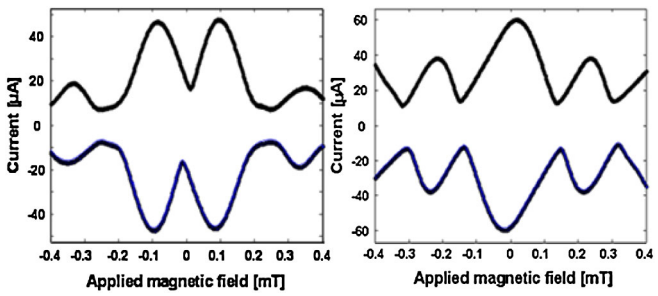

FIG. 2 (color online). Critical current as a function of externally applied magnetic field for the 0-π junction (left panel) and the 0 junction (right panel) at $T = 40$ K. The two plots show the expected complementary behavior between the 0-π junction and the reference 0 junction. The slightly slanted pattern is a result of self-field effects.

junctions were about the same size as the SQUID pickup loop, the spontaneous magnetization in the junctions was relatively small, and interaction between the SQUID pickup loop and the sample caused switching of the semifluxon sign while scanning. Nevertheless, we observed spontaneous magnetization in the junction region for the 0-π junctions that was not present in the corresponding 0 junctions. SSM cross sections for one pair of 0 and 0-π junctions are given in Fig. 3(b). Figure 3(a) shows a cartoon of the two junctions based on an optical image. The dotted lines indicate where the data points shown in Fig. 3(b) were collected. For each junction, the line along the GB is plotted after subtraction of the line behind the GB to remove a background. When the flux is plotted as a function of the position for the 0-π junction, a flux signal is found that is absent in the 0 junction.

The spontaneous flux generated at the corner of the 0-π junction of Fig. 3 was determined by a numerical solution of the sine-Gordon equation for the specific grain boundary configuration [19]. The flux through the SQUID pickup was numerically integrated assuming a pickup loop height of 1.4 μm, from fits to images of bulk vortices [26]. The calculated peak flux signal Φ is $\Phi/\Phi_0 = 0.1$, compared with the measured signal $\Phi/\Phi_0 = 0.03$. We attribute this difference to the effect of microfaceting along the GB caused by the morphology of the YBCO films [27]. Microfaceting reduces the spontaneous flux since if the GB angle for the microfacet strongly deviates from the nominal angle, the sign of the critical current density may change, reducing the total phase change along the junction. Although an estimation of the facet length, GB angles and relative phase for the facets from AFM images show that the reduction of the magnetic flux compared to the expected signal is consistent with microfaceting, an exact calculation of the expected signal is not possible since we cannot unambiguously determine the critical current density from the morphology of the GB. It is worth noting that we detected semifluxons with a signal Φ/Φ_0 varying

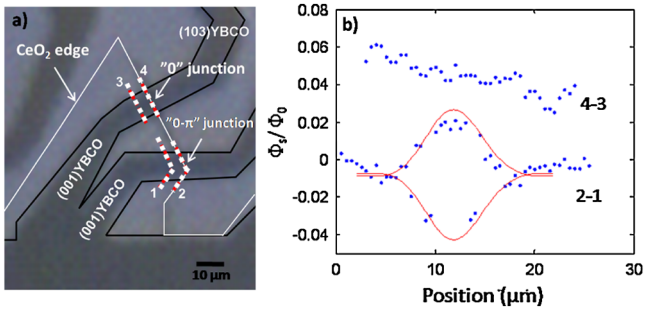

FIG. 3 (color online). (a) Sketch of two of the junctions that were imaged with the SSM. (b) The flux signal plotted as a function of position [as indicated in (a)] for the 0-π junction and the 0 junction, respectively. The SSM signals (dots) agree well with modeling (solid line) when faceting is accounted for. Both positive and negative flux values occur along the GB line for the 0-π junction because of flipping of the semifluxon during scanning.

between 0.025 and 0.036 in 5 more 0-π junctions with GB angles in the range between 10° and 30° (data not shown). No semifluxons were found in the corresponding 0 junctions. This fact further confirms that we indeed observe the nucleation of semifluxons in our 0-π junctions and not random trapped magnetic flux close to the GB.

A semifluxon at the corner of a long 0-π junction manifests itself in the phase dynamics of the junction through Fiske steps and zero-field steps (ZFSs) in the current-voltage (IV) characteristic. ZFSs appear at different voltage values for a 0-π junction compared to a 0 junction [20,28,29]. We have observed both kinds of resonance steps in our devices.

The Fiske steps, which appear at finite magnetic field, are the result of the junction acting as a transmission line [30]. They appear at voltages $V_n^F = \frac{n\Phi_0\bar{c}}{2L}$, where $\bar{c}$ is the Swihart velocity and n is an integer that determines the number of wavelengths composing a standing electromagnetic wave. ZFSs appear only in long junctions and occur, in contrast to Fiske steps, in the absence of magnetic field. They are the result of fluxons (solitons) traveling along the junction. In an ideal junction, a fluxon will be reflected at the end of the junction and travel back as an antifluxon. Such a cycle is completed in $t = \frac{2L}{\bar{c}}$ and is associated with a total flux evolution of $2\phi_0$. The ZFSs will consequently occur at voltages

$$V_n^{\mathrm{ZFS}} = \frac{n\Delta\Phi}{\Delta t} = \frac{n\Phi_0\bar{c}}{L} \tag{1}$$

where n is an integer corresponding to the number of fluxons moving in the Josephson junction. ZFSs are hence found at twice the spacing as Fiske steps.

In a 0-π junction with a semifluxon at the discontinuity point, the traveling fluxons interact with the semifluxon, making it flip polarity, resulting in an additional π-phase change during the same time period. As a result, the steps occur at voltages given by Eq. (1) where $n = N + 1/2$, N an integer (half integer ZFS's). In the ideal case, the first half integer ZFS occurs as a result of the semifluxon flipping polarity twice during one period in the junction. The second half integer ZFS also includes a fluxon-antifluxon pair [31].

Figure 4 presents the current through the 0 and 0-π junction at a GB angle of 20° as a function of external field for various fixed bias voltages. For both junctions, ZFSs are found. In the 0-π junction, the first (half integer) ZFS is found at the same voltage (around 0.4 mV) as the first Fiske step [see Fig. 4(a)]. For the 0 junction, the first ZFS is found at twice the voltage (1 mV) of the first FS (0.5 mV), as shown in Fig. 4(b). However, our junctions are not ideal, having both an appreciable dissipation and an asymmetric current distribution. The ZFSs appear at a small finite field due to self-fields generated by the Josephson current. The ZFSs occur when the external magnetic fields exactly cancel out the intrinsically generated ones.

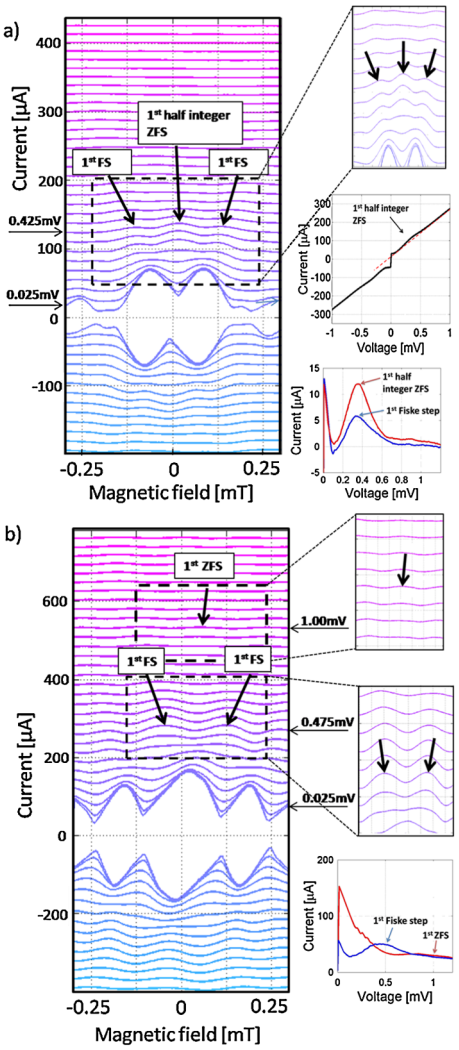

FIG. 4 (color online). Dependence of the current on external magnetic field at fixed voltages, with intervals of 0.05 mV, for a 0-π junction (a) and 0 junction (b). Resonances are indicated by arrows. Relatively high dissipation in the junction leads to broad resonant steps in the IV curve, and steps over a broad voltage range in the voltage contour plots.

In this respect, we performed simulations of the phase dynamics $\varphi(x, t)$ by solving numerically the sine-Gordon equation for 0- and 0-π junctions using homogeneous critical current distributions along the GB line [19]. Deviations from perfect symmetry of the critical current distribution were modeled by introducing asymmetric boundary conditions. Figures 5(a) and 5(b) shows the voltage contours extracted from the simulations using $L/\lambda_j = 3$, the dissipation parameter $\alpha = 1/Q = 1/\omega_p RC \approx 0.75$ (adjusted to reproduce the experimental results), where $\omega_p = \sqrt{2\pi I_0/C\phi_0}$ is the plasma frequency, I_0 is the critical current, C the capacitance, and R is the normal resistance of the junction. The ratio of the measured magnetic field periodicity between the 0-π and 0 junction is 1.4 instead of 2 (see Fig. 2), which one would expect for a uniform critical current distribution along the

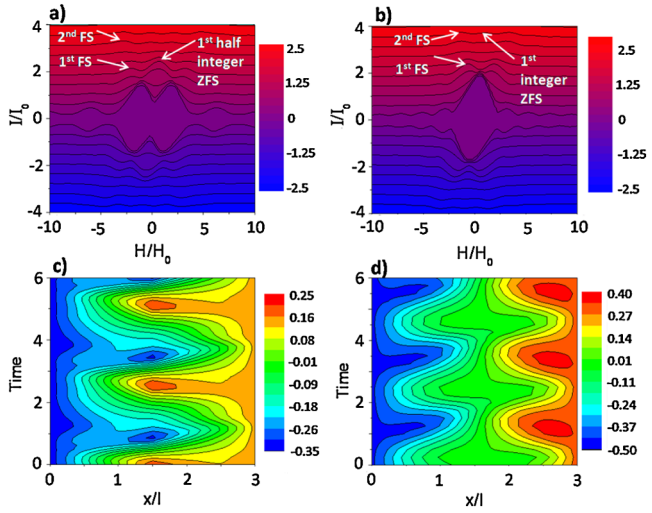

FIG. 5 (color online). Numerical simulations showing constant voltage contours (in a.u.) for a 0-π junction (a) and a 0 junction (b) with the dissipation parameter $\alpha = 0.75$ and the junction length $L/\lambda_j = 3$. The arrows indicate Fiske and zero-field steps. H/H_0 is the normalized applied magnetic field, $H_0 = 2\lambda_j J_c$, and J_c is the critical current density. Local magnetic flux (a.u.) in a 0-π junction (c) and a 0 junction (d) as a function of time (normalized to the plasma frequency) and position along the length of the junction. Note that the positive and negative semifluxon fields in Fig. 5(c) have different values due to asymmetric boundary conditions.

GB [see Figs. 5(a) and 5(b)]. This difference can be attributed to faceting along the GB line, which can strongly alter the periodicity of the magnetic field pattern [32,33], consistent with our results.

In Figs. 5(c) and 5(d), we show the dynamics of the local magnetic field (local derivative of phase) at the first ZFS. Figure 5(c) shows the simulated dynamics for the 0-π junction. During half a period $\Delta t = L/\bar{c}$, a fluxon enters the junction and flips the semifluxon in the center. During the next half period, an antifluxon enters the junction from the other side, moves to the center, and flips the semifluxon again. In the full period $\Delta t = 2L/\bar{c}$, we obtain a flux change of $1\Phi_0$. This corresponds to the voltage position of the first half integer ZFS ($n = 1/2$). For the 0-junction [Fig. 5(d)], during each period a fluxon and an antifluxon enter the junction from opposite sides and annihilate at the center of the junction. The asymmetry of the junction causes the two fluxons to propagate only to the center instead of crossing the whole length of the junction. The total flux change during one period $\Delta t = L/\bar{c}$ is $1\Phi_0$, resulting in a voltage position of the current step corresponding to the first ZFS according to Eq. (1). The simulations show that the ZFSs are dominated by the dynamics of fluxons, for integer ZFS in 0 junctions, and by the interaction of fluxons and semifluxons for the half integer ZFS in 0-π junctions.

To conclude, in our experiment, the detection of a static semifluxon by SSM allows the correlation between the dynamics of the system and the interaction between fluxon and semifluxon. The biepitaxial technique allows the fabrication on the same chip of topologically different semifluxon configurations with different ground state energies simply by varying the grain boundary angle. This might be a great advantage in dealing with the manipulation of semifluxons in digital logic. At the same time, our junctions have shown a macroscopic degree of freedom [34,35], which is a promising step towards the goal of operating semifluxons in the quantum regime.

This work has been partially supported by the Swedish Research Council (VR), EU STREP project MIDAS, the Knut and Alice Wallenberg Foundation.

[1] L. N. Bulaevskii, V. V. Kuzii, and A. A. Sobyanin, JETP Lett. **25**, 290 (1977).
[2] A. V. Andreev, A. I. Buzdin, and R. M. Osgood, Phys. Rev. B **43**, 10124 (1991).
[3] A. Bauer *et al.*, Phys. Rev. Lett. **92**, 217001 (2004).
[4] H. Hilgenkamp, Supercond. Sci. Technol. **21**, 034011 (2008).
[5] D. A. Wollman *et al.*, Phys. Rev. Lett. **71**, 2134 (1993).
[6] C. C. Tsuei *et al.*, Phys. Rev. Lett. **73**, 593 (1994).
[7] T. Ortlepp *et al.*, Science **312**, 1495 (2006).
[8] V. B. Geshkenbein, A. I. Larkin, and A. Barone, Phys. Rev. B **36**, 235 (1987).
[9] M. Sigrist and T. M. Rice, J. Phys. Soc. Jpn. **61**, 4283 (1992).
[10] D. A. Wollman *et al.*, Phys. Rev. Lett. **74**, 797 (1995).
[11] H. Hilgenkamp *et al.*, Nature (London) **422**, 50 (2003).
[12] J. R. Kirtley *et al.*, Nature (London) **373**, 225 (1995).
[13] J. R. Kirtley *et al.*, Nature Phys. **2**, 353 (2006).
[14] T. V. Rajeevakumar *et al.*, Phys. Rev. B **21**, 5432 (1980).
[15] T. Kontos *et al.*, Phys. Rev. Lett. **89**, 137007 (2002).
[16] A. A. Bannykh *et al.*, Phys. Rev. B **79**, 054501 (2009).
[17] M. Weides, Appl. Phys. Lett. **93**, 052502 (2008).
[18] J. H. Xu, J. H. Miller, and C. S. Ting, Phys. Rev. B **51**, 11958 (1995).
[19] J. R. Kirtley, K. A. Moler, and D. J. Scalapino, Phys. Rev. B **56**, 886 (1997).
[20] J. Pfeiffer *et al.*, Phys. Rev. B **77**, 214506 (2008).
[21] E. Goldobin *et al.*, Phys. Rev. Lett. **92**, 057005 (2004).
[22] F. M. Granozio *et al.*, Phys. Rev. B **67**, 184506 (2003).
[23] F. Lombardi *et al.*, Phys. Rev. Lett. **89**, 207001 (2002).
[24] Y. Zuev, M. S. Kim, and T. R. Lemberger, Phys. Rev. Lett. **95**, 137002 (2005).
[25] J. Johansson *et al.*, Phys. Rev. B **79**, 214513 (2009).
[26] J. R. Kirtley *et al.*, Phys. Rev. Lett. **76**, 1336 (1996).
[27] F. Tafuri *et al.*, Phys. Rev. B **59**, 11523 (1999).
[28] N. Lazarides, Phys. Rev. B **69**, 212501 (2004).
[29] N. Stefanakis, Phys. Rev. B **66**, 214524 (2002).
[30] A. Barone and G. Paterno, *Physics and Applications of the Josephson Effect* (Wiley-VCH, New York, 1982).
[31] G. Rotoli *et al.* (unpublished).
[32] H. J. H. Smilde *et al.*, Phys. Rev. Lett. **88**, 057004 (2002).
[33] T. Lindstrom *et al.*, Phys. Rev. B **74**, 014503 (2006).
[34] T. Bauch *et al.*, Science **311**, 57 (2006).
[35] T. Bauch *et al.*, Phys. Rev. Lett. **94**, 087003 (2005).